

# Multiscale Sparsifying Transform Learning for Image Denoising

Ashkan Abbasi<sup>a</sup>, Amirhassan Monadjemi<sup>b,\*</sup>, Leyuan Fang<sup>c,\*</sup>, Hossein Rabbani<sup>d</sup>, and Neda Noormohammadi<sup>a</sup>.

<sup>a</sup> Artificial Intelligence Department, Faculty of Computer Engineering, University of Isfahan, Isfahan, Iran.

<sup>b</sup> School of Continuing and Lifelong Education, National University of Singapore, Lower Kent Ridge Road, Singapore. (E-mail: [sleam@nus.edu.sg](mailto:sleam@nus.edu.sg))

<sup>c</sup> College of Electrical and Information Engineering, Hunan University, Changsha, China. (E-mail: [fangleiyuan@gmail.com](mailto:fangleiyuan@gmail.com))

<sup>d</sup> Department of Biomedical Engineering, Medical Image and Signal Processing Research Center, School of Advanced Technologies in Medicine, Isfahan University of Medical Sciences, Isfahan, Iran.

Asterisk indicates the corresponding author.

**Abstract**—The data-driven sparse methods such as synthesis dictionary learning and sparsifying transform learning have been proven to be effective in image denoising. However, these methods are intrinsically single-scale, which ignores the multiscale nature of images. This often leads to suboptimal results. In this paper, we propose several strategies to exploit multiscale information in image denoising through the sparsifying transform learning denoising (TLD) method. To this end, we first employ a simple method of denoising each wavelet subband independently via TLD. Then, we show that this method can be greatly enhanced using wavelet subbands mixing, which is a cheap fusion technique, to combine the results of single-scale and multiscale methods. Finally, we remove the need for denoising detail subbands. This simplification leads to an efficient multiscale denoising method with competitive performance to its baseline. The effectiveness of the proposed methods are experimentally shown over two datasets: 1) classic test images corrupted with Gaussian noise, and 2) fluorescence microscopy images corrupted with real Poisson-Gaussian noise. The proposed multiscale methods improve over the single-scale baseline method by an average of about 0.2 dB (in terms of PSNR) for removing synthetic Gaussian noise from classic test images and real Poisson-Gaussian noise from microscopy images, respectively. Interestingly, the proposed multiscale methods keep their superiority over the baseline even when noise is relatively weak. More importantly, we show that

*the proposed methods lead to visually pleasing results, in which edges and textures are better recovered. Extensive experiments over these two different datasets show that the proposed methods offer a good trade-off between performance and complexity.*

*Index Terms— Sparsifying Transform Learning, Multiscale Sparse Representations, Wavelets, Natural Image Denoising, Fluorescence Microscopy Denoising (FMD).*

## 1. Introduction

The random noise is inherent in any imaging system, which originates from various sources such as the physics of circuits, nature of the image formation, and environmental conditions. Regardless of its origin, noise causes random intensity variations which degrade the visual quality and negatively affect higher-level computer vision tasks. Thus, image denoising is an important low-level vision task with various applications. The main goal is to simultaneously remove noise, preserve the sharpness of edges, and suppress undesirable artifacts. Since this problem is ill-conditioned, the model used for underlying image or noise plays a central role in regularizing the process of denoising.

Sparse models have been proven to be effective in various image restoration and compression problems. Two well-known approaches to exploit the notion of sparsity are fixed transform models (such as discrete cosine transform (DCT) [1] and wavelets [2]) and synthesis sparse models [3–5]. A fixed transform decomposes an image through a fixed set of analysis filters into sparse representations. Then, a corresponding set of synthesis filters is used to reconstruct the image back from its representations. These analysis and synthesis filters are derived based on a mathematical model of the data and desired characteristics, leading to highly structured transforms with fast implementations. In practice, while fixed transform models are fast (due to simplicity of sparse coding step), data-driven synthesis sparse models are more powerful (in terms of representation capacity). This representation power mainly comes from using data-driven dictionaries instead of fixed ones. To enjoy both simplicity of sparse coding and adaptivity to data, Ravishanker and Bressler [6–8] pioneered the sparsifying transform learning model. They have shown that their model has comparable or even better performance compared to the well-known K-SVD synthesis dictionary learning [4,5].

Images are naturally composed of features at different scales. Ignoring the multiscale nature of images in a model used for solving an image denoising problem can lead to suboptimal estimates. In [9], it is reported that most well-known denoising methods focus on removing noise from high-frequency contents and leave low-frequency noise, leading to considerable artifacts and low-frequency content loss. Especially, the appealing of multiscale denoising increases when noise is not weak. In some fixed sparse models such as wavelets, multiscale processing is inherent. However, the well-known adaptive or learning based sparse models such as synthesis dictionary learning [4,5] and sparsifying transform learning [6–8] are intrinsically single-scale.

There are promising efforts to integrate multiscale analysis with data-driven sparse models [10–18]. The idea of learning sparse multiscale image representations dates back to the works of Olshausen et al. [10,11]. They show how a wavelet basis can be adapted to the statistics of natural images, and achieve slightly better coding efficiency [10] and denoising [11] compared to using some fixed basis transforms. But these methods are fairly elaborate and computationally demanding since they rely on the sampling techniques to infer sparse codes. In [13], K-SVD is extended to simultaneously use different sizes of atoms, each size corresponding to a different scale. Then, dictionary learning is carried out in a way to update each atom in each scale. This method leads to very promising results, though it is computationally expensive. It also does not benefit from the information provided by the coarse-scale image, obtained by sub-sampling the input image, which contains substantial low-frequency information [9].

In a different approach, data-driven sparse models are directly applied in the multi-resolution analysis domain [12–18]. In this way, the frequency selectivity of wavelet subbands acts as a divide and conquer strategy which could result in sparser representations and simplify further processing. In [12], a method based on filtering principal component coefficients of wavelet packet subbands is presented. This method ignores filtering the approximate subband and is based on non-adaptive shrinkage methods which leaves a considerable amount of noise and artifacts. Ophir et al. [14] have successfully shown that the K-SVD denoising method [5] can be utilized to efficiently filter wavelet subbands. In their proposed multi-scale K-SVD (MS K-SVD) method, separate adaptive dictionaries are learned to denoise the approximate and detail subbands. Their experiments show that MS K-SVD partially outperforms plain KSVD, especially when noise is relatively strong. Generally, MS K-SVD recovers textures, edges and main image structures better than the plain K-SVD denoising method. However, its results suffer from artifacts [16–18]. This is because MS K-SVD does not consider the overall consistency between wavelet subbands, i.e., each wavelet subband is denoised independent of the others.

Later, the approach of directly applying data-driven sparse models in the multi-resolution analysis domains is exploited further in [15,16]. They basically try to enrich this approach by utilizing other techniques such as structural clustering and nonlocal self-similarity. In [18], a fully Bayesian statistical approach is presented to learn a single dictionary in the domain of the Laplacian pyramid [19]. This dictionary is shared across scales, and thus helps to reduce the computational cost. While promising results have been reported, sharing one dictionary across scales may be sub-optimal. In [17], a joint sparse representation based strategy is exploited to combine the results of the plain K-SVD [5] and MS K-SVD [14] denoising methods. The assumption is that the underlying structure between these two results are the same. Therefore, the joint sparse representation [20] can be used to recover the underlying image without artifacts. Although the artifacts are suppressed greatly, the computational cost increases significantly since the joint sparse representations are obtained using concatenated input vectors and dictionaries.

In this work, we propose several strategies to integrate data-driven sparse models and multiscale analysis. Although most efforts have been made in enriching the data-driven synthesis sparse models with multi-scale analysis [13–18], we use sparsifying

transform learning [6–8] which has convergence guarantee and computational advantages compared to synthesis sparse models [3–5]. We first apply an adaptive transform learning denoising method [6] to denoise each wavelet subband. When all wavelet subbands (the approximate and detail subbands) are denoised, the inverse wavelet transform can be computed to obtain an estimate of the noise free image. Compared to directly denoising the corrupted image, image details are better recovered by processing its wavelet subbands. However, the results suffer from artifacts which considerably degrade the overall denoising quality. We experimentally analyze the shortcomings of this approach, and then two other strategies based on the wavelet subbands mixing technique [21,22] are proposed which significantly improve the quality of results. In short, we first combine the results of single-scale and multi-scale denoising methods. This technique greatly suppresses undesirable artifacts while, unlike the sparsity based fusion method in [17], it is not computationally expensive. However, the whole method is still computationally demanding since it needs to denoise all wavelet subbands. We then show that using the same kind of wavelet transform in both of the denoising and mixing stages greatly simplifies our method and yields to a new multiscale denoising method in which there is no need to explicitly denoise detail subbands. This property allows us to save the computational cost of denoising detail subbands. Moreover, the proposed method is simpler since there is no need to adjust hyper-parameters of the method which is used for denoising detail subbands.

All of the proposed methods are comprehensively examined over two different sets of images: 1) classic test images, and 2) fluorescence microscopy images. The former set of images is corrupted with synthetic additive white Gaussian noise and the latter is inherently corrupted with real Poisson-Gaussian noise. In the past few years, the application of image denoisers to real noisy images has attracted attentions [23–26]. Thus, we show the effectiveness of the proposed methods to remove real noise from fluorescence microscopy images [25]. Our experiments show that since there are various small patterns and textures in microscopy images, the multiscale denoising is advantageous. A property of our proposed multiscale mixing based methods is that the quality of denoising is preserved even when noise is relatively weak. The overall qualitative and quantitative comparisons reveal that the proposed methods offer a good trade-off between performance and complexity.

The rest of this paper is organized as follows. In the following section, we briefly review related works. Next, we describe the proposed multi-scale methods in Section 3. The experimental results are presented in Section 4, and the paper concludes in Section 5.

## 2. Related Works

### 2.1 Sparsifying Transform Learning

Transform models [6–8] assumes that signals of interest can be approximately sparsifiable using a transform matrix  $W \in \mathbb{R}^{m \times n}$ , i.e.  $Wy = x + e$ , where  $y \in \mathbb{R}^n$  is a signal vector,  $x \in \mathbb{R}^m$  is the sparse codes of the signal, and  $e \in \mathbb{R}^m$  is the modeling error. In

this model, given a signal  $y$  and transform  $W$ , the sparse coding problem is defined as minimization of  $\|Wy - x\|_2^2$  with respect to  $x$  subject to  $\|x\|_0 \leq \tau$ , where  $\tau$  is a given sparsity level. The exact solution is easily obtained by thresholding  $Wy$  to the  $\tau$  largest magnitude coefficients.

To learn a transform  $W$  from data, given a matrix of  $N$  training signals  $Y \in \mathbb{R}^{n \times N}$ , we can minimize the sparsification error defined as  $\|WY - X\|_F^2$  with respect to both  $W$  and  $X$ , subject to sparsity of  $X$ . However, unless a suitable regularization is imposed on  $W$ , the learned transform has poor performance. In [6], the following formula for learning a well-conditioned square transform  $W$  ( $m = n$ ) is proposed:

$$\min_{W, X} \|WY - X\|_F^2 + \lambda Q(W) \text{ s.t. } \|X_i\|_0 < \tau \quad \forall i \quad (1)$$

where,  $Q(W) = -\log|\det W| + \mu\|W\|_F^2$  is a regularizer to prevent trivial solutions. The  $-\log|\det W|$  penalty is imposed to avoid singular solutions, and the  $\|W\|_F^2$  penalty prevents the loss function from being unbounded below.

To solve (1), an alternating optimization algorithm is proposed in [6]. This procedure alternates between sparse coding step and transform update step. Both iterative [6] and closed-form [8] solutions are presented for the transform update step. Here, we employ the closed-form solution which is faster and has a global convergence guarantee.

## 2.2 Image Denoising via Sparsifying Transform Learning

Given a transform  $W$  and sparse code  $x$ , the least squares estimate of the underlying signal vector  $u$  is obtained using  $\hat{u} = W^\dagger x$ , where  $W^\dagger$  denotes pseudoinverse of  $W$ . Ideally, in the transform model, corruptions such as noise cannot be well approximated in the transform domain, thus finding the sparse code of a corrupted signal over a suitable transform helps to restore it. Based on this fact, in [6], an adaptive signal denoising method using sparsifying transform learning is proposed by adding a data fidelity term to (1):

$$\begin{aligned} \min_{W, X, \hat{U}} & \|WY - X\|_F^2 + \lambda Q(W) + \tau \|Y - \hat{U}\|_F^2 \\ \text{s.t. } & \|X_i\|_0 < \tau_i \quad \forall i \end{aligned} \quad (2)$$

where  $Y \in \mathbb{R}^{n \times N}$  is a matrix whose columns represent  $N$  signals corrupted by additive white Gaussian noise, and  $\hat{U} \in \mathbb{R}^{n \times N}$  is a matrix containing recovered signals. The parameter  $\tau$  is chosen inversely proportional to noise level  $\sigma$ .

To use the above formula for image denoising, the observed image  $Y$  is first divided using  $R_i y$  into small overlapping patches of size  $\sqrt{n} \times \sqrt{n}$ , with  $R_i$  being the patch extraction operator and  $y$  being the vector form of image. Then, the mean intensity of each patch is removed, and all extracted patches  $Y_i = R_i y$  are arranged as columns of matrix  $Y$ . Next, the problem (2) can be solved using an alternating optimization algorithm. The procedure alternates between a transform learning step and a variable sparsity update step. The transform learning step itself is composed of a sparse coding step (with fixed sparsity levels) and a transform update step. Both of these steps are solved using closed-form solutions [8]. However, it turns out that using fixed sparsity levels

degrade denoising performance. Therefore, an efficient variable sparsity update step is also proposed in [6,7]. For fixed  $W$  and  $X_i$  ( $i = 1, 2, \dots, N$ ), this step reduces to the least squares problem in the  $\hat{U}_i$ 's. Each  $\hat{U}_i$  is updated by adding one nonzero element at a time from  $WY_i$  to  $X_i$ , until the error measure  $\|Y_i - \hat{U}_i\|$  falls below a given threshold  $nc^2\sigma^2$ ; where  $c$  is a fixed parameter. Finally, when all the estimated patches  $\hat{U}_i$  are recovered, the denoised image  $\hat{U}$  can be obtained by adding back the mean intensities to the final estimates and averaging them at their respective locations in the image.

### 3. The Proposed Methods

The sparsifying Transform Learning Denoising (TLD) [6–8] is briefly reviewed in Section 2.2. In this section, we propose three procedures which can be used to make TLD multiscale. First, inspired by the works reported in [14,17], we use TLD to denoise each wavelet subband. We refer to this method as the Multiscale TLD (MTLD) which is our first proposed multiscale extension for TLD. Then, by emphasizing on the shortcomings of this approach, more effective methods are developed which are based on combining the results of TLD and MTLD.

To derive the proposed MTLD method, we begin by applying an analytical transform to data matrix  $Y$  in the formula of sparsifying transform learning (1). Let the transform matrix  $W$  in (1) be the product of two different square transforms  $B\Phi$ , then:

$$\min_{B, X} \|B\Phi Y - X\|_F^2 + \lambda Q(B) \text{ s.t. } \|X_i\|_0 < \tau \quad \forall i \quad (3)$$

where,  $\Phi$  is an efficient fixed analytical transform, and  $B$  is a transform that is to be learned from data.

To solve (3), in [7], the authors suggest to simultaneously encourage transform  $B$  and sparse code  $X$  matrices to be sparse. This formulation is called the doubly sparse transform learning and is solved using iterative nonlinear conjugate gradients. However, here we do not encourage  $B$  to be sparse because: (i) Although the doubly sparse formulation is successful in the synthesis sparse model [27], it is experimentally shown in [7] that this notion restricts modeling capability and slightly affects denoising results when it is used with the sparsifying transform model, (ii) If we encourage sparsity of the transform matrix  $B$ , the efficient closed-form solution for the transform update step [8] cannot be used, and (iii) The doubly sparse formulation works well when it is used with an analytical transform such as DCT, for which the transform matrix can be directly applied to data. In the case of multiscale transforms such as wavelets, transform matrices are relatively large, and therefore it is not straightforward to use the doubly sparse formulation with large transform matrices. Instead, a more intuitive and simpler approach can be taken by learning a separate transform  $B_s$  for each wavelet subband [14]:

$$\begin{aligned} \min_{B_s, X_s} & \|B_s(\Phi Y)_s - X_s\|_F^2 + \lambda Q(B_s) \\ \text{s.t. } & \|X_{s_i}\|_0 < \tau \quad \forall i, \forall s \end{aligned} \quad (4)$$

where subscript  $s$  indicates different wavelet subbands, and  $(\Phi Y)_s$  denotes a matrix containing signal vectors of the  $s$ -th wavelet subband. The above formula is similar to (1) except that it learns multiple separate transforms from all wavelet subbands. Therefore,

it suggests that we can use TLD for denoising each wavelet subband. The proposed MTLT method is developed based on this fact and its flowchart is shown in Fig. 1(a). MTLT first applies a  $J$ -scale wavelet transform to the input image  $\mathbf{Y}$  and then decomposes it into a set of wavelet subbands  $\mathcal{S} = \{\mathbf{A}^J, \mathcal{D}^J\}$ , where  $\mathbf{A}^J$  and  $\mathcal{D}^J$  represent the approximate subband at scale  $J$  and a set containing all of detail subbands at different scales, respectively. Next, the patches of each wavelet subband is extracted and denoised through TLD that takes three inputs: noisy wavelet subband ( $\mathcal{S}$ ), patch size ( $p$ ), and standard deviation of noise ( $\sigma_S$ ) in the input image. Finally, all of the denoised wavelet subbands are used to compute the inverse wavelet transform and reconstruct the estimated denoised image  $\hat{\mathbf{X}}_M$ . MTLT provides a simple way to incorporate multiscale information in the denoising procedure. However, in practice, we found that it leads to generally inferior results compared to its baseline (TLD). As an example, the results of denoising a test image with TLD and MTLT are shown in Fig. 2 (c) and (d). The corresponding zoomed regions from these images are shown in Fig. 2 (i) and (j), respectively. These visual results confirms that although the main image structures (or low-frequency information) are better recovered through MTLT, the presence of relatively strong artifacts in MTLT's output negatively affect the quality of denoising. In this example, the artifacts in the Fig. 2 (j) are better observed by zooming on a computer screen. The presence of these artifacts are also resulted in the lower value of the Peak Signal-to-Noise-Ratio (PSNR) compared to the PSNR of TLD. This weakness of the proposed MTLT method can be explained by the fact that MTLT denoises each wavelet subband independently, and without considering the consistency between wavelet subbands. Furthermore, denoising each wavelet subband using TLD may need careful parameter adjustment for each wavelet subband, which is a quite cumbersome procedure.

As experimentally shown in the above example, while the result of MTLT suffer from considerable artifacts (or unwanted high frequency components), the result of TLD do not suffer from high frequency artifacts. In fact, the single-scale TLD method can effectively remove high frequency noise, but it also removes prominent image structures and degrades low frequency contents. To overcome these shortcomings and reconstruct a higher quality image, we propose to exploit the wavelet subbands mixing technique [21], [22] in order to combine the best of both methods: (i) The main image structure and low frequency contents of the proposed MTLT result, and (ii) The high frequency contents of the TLD result. We call this method the Mixed MTLT (MMTLT) method, because it is based on mixing outputs of the TLD and proposed MTLT methods. The flowchart of the proposed MMTLT method is shown in Fig. 1(b), and it is summarized as follows. First, the outputs of TLD ( $\hat{\mathbf{X}}_S$ ) and MTLT ( $\hat{\mathbf{X}}_M$ ) are separately decomposed using a  $K$ -scale wavelet transform into their approximate and detail subbands. Then, a new set ( $\hat{\mathcal{S}}_X$ ) of wavelet subbands is created from the approximate subband ( $\hat{\mathbf{A}}_M^K$ ) of the proposed MTLT output and the set of all detail subbands ( $\hat{\mathcal{D}}_S^K$ ) of the TLD output. Finally, the inverse wavelet transform is computed on the set ( $\hat{\mathcal{S}}_X$ ) of mixed wavelet subbands to reconstruct the final estimated denoised image ( $\hat{\mathbf{X}}_{MM}$ ). In the proposed MMTLT method (Fig. 1(b)), two different wavelet transforms are used. The first one is the  $J$ -scale wavelet transform (denoted by "WT" in Fig. 1(a)) that is used to decompose the input image ( $\mathbf{Y}$ ), and the second one is a  $K$ -scale wavelet transform (denoted by "WTX" in Fig. 1(b)) that is applied two times in the mixing stage of MMTLT. These

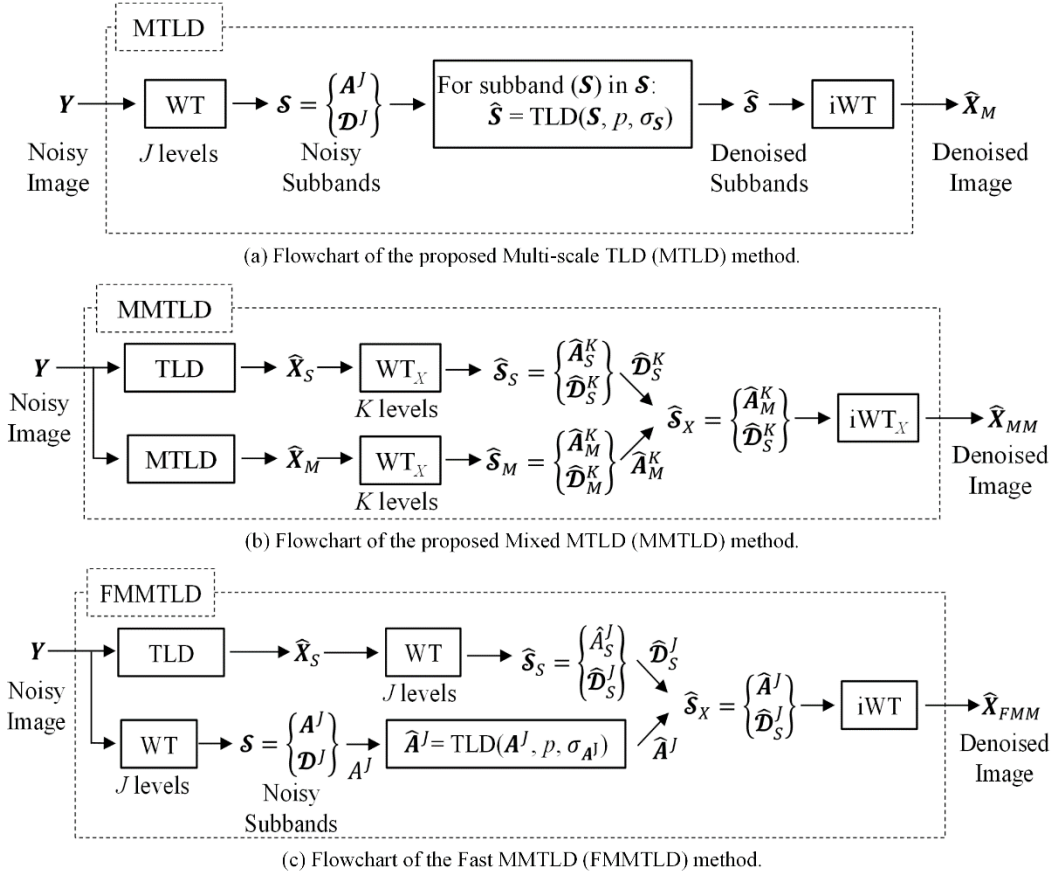


Fig. 1: Flowcharts of the proposed multiscale sparsifying transform learning denoising (TLD) methods: (a) The multiscale TLD (MTLD) is developed exactly based on [14], except here we use TLD instead of K-SVD denoising. MTLD serves as our baseline method. In (b) and (c), the two other proposed multiscale denoising methods (MMTLD and FMMTLD) are shown. These methods are the main contributions of this paper. The “WT” and “WT<sub>X</sub>” modules show a  $J$ -scale and a  $K$ -scale wavelet transforms, respectively. The corresponding inverse wavelet transforms are shown with “iWT” and “iWT<sub>X</sub>”.

two wavelet transforms (“WT” and “WT<sub>X</sub>”) are independent of each other. We can select appropriate wavelet transforms for each of the denoising and mixing stages, respectively. However, when these two wavelet transforms are selected to be the same (i.e., the same filter bank and the same number of decomposition levels ( $J = K$ )), considerable amount of computations can be saved. This is because the set of detail subbands ( $\hat{\mathcal{D}}_M^K$ ) is discarded in the mixing stage of the proposed MMTLD method. Therefore, when these two wavelet transforms are the same, denoising detail subbands in MTLD becomes redundant. To see why this is the case, consider that the last step of MTLD is the application of the inverse wavelet transform (“iWT”) to the set of denoised wavelet subbands ( $\hat{\mathcal{S}}$ ). Then, the output of MTLD ( $\hat{\mathcal{X}}_M$ ) is transformed again using another wavelet transform (“WT<sub>X</sub>”) to decompose it into a set of wavelet subbands ( $\hat{\mathcal{S}}_M$ ). When “WT” is selected to be the same wavelet transform as “WT<sub>X</sub>”, these two sets of wavelet subbands become equal ( $\hat{\mathcal{S}} = \hat{\mathcal{S}}_M$ ). In the next step, MMTLD only uses the approximate subband ( $\hat{\mathcal{A}}_M^K$ ) and discards the set of detail subbands ( $\hat{\mathcal{D}}_M^K$ ). Therefore, it is not necessary to denoise detail subbands. This property allows us to save redundant computations and leads to a more computationally efficient method. In this base, we propose the Fast MMTLD (FMMTLD) method. It is equivalent to MMTLD if the same kind of wavelet transform is used in the denoising and mixing stages. The flowchart



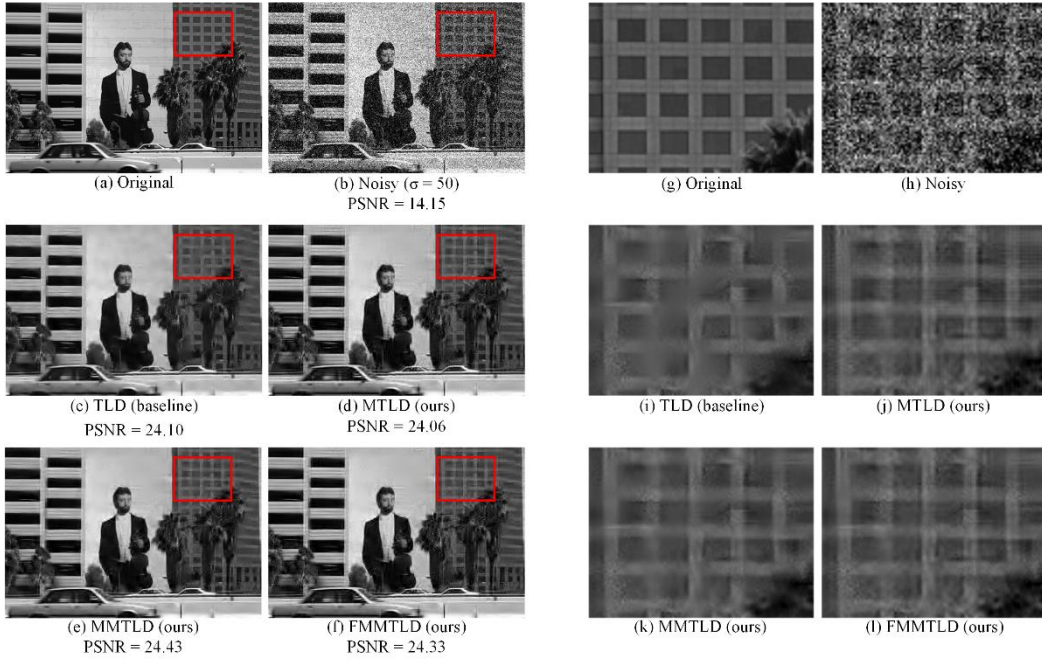


Fig. 2: Visual comparison of denoising results by the base line TLD method and the proposed multiscale methods (MTLD, MMTLD, and FMMTLD). The original image is ‘test011’ from the BSD68 dataset.

of the proposed FMMTLD method is shown in Fig. 1(c) which shows that it consists of two branches. The first branch is aimed at obtaining a set of denoised detail subbands ( $\hat{\mathcal{D}}_S^J$ ). This is done indirectly, where the input image ( $\mathbf{Y}$ ) is denoised using TLD and then a  $J$ -scale wavelet transform (“WT”) is applied to the output of TLD ( $\hat{\mathbf{X}}_S$ ) to decompose it into a set of wavelet subbands ( $\hat{\mathcal{S}}_S$ ). From this set, the set of detail subbands ( $\hat{\mathcal{D}}_S^J$ ) are kept and the approximate subband ( $\hat{\mathcal{A}}_S^J$ ) is discarded. Instead of ( $\hat{\mathcal{A}}_S^J$ ), FMMTLD uses the second branch’s output which is obtained as follows. The input image ( $\mathbf{Y}$ ) is decomposed into the noisy wavelet subbands ( $\mathcal{S}$ ), and then only the approximate subband ( $\mathcal{A}^J$ ) is directly denoised. Once the denoised approximate subband ( $\hat{\mathcal{A}}^J$ ) and the set of denoised detail subbands ( $\hat{\mathcal{D}}_S^J$ ) are ready, a new set ( $\hat{\mathcal{S}}_X$ ) of wavelet subbands is formed. Finally, the inverse wavelet transform is computed to reconstruct the estimated denoised image ( $\hat{\mathbf{X}}_{FMM}$ ).

Comparing the flowchart of FMMTLD (Fig. 1(c)) and MMTLD (Fig. 1(b)) reveals that FMMTLD saves two inverse wavelet transforms and, more importantly, it saves operations needed to denoise all detail subbands. Considering the fact that the bottleneck of MTLD and MMTLD are denoising wavelet subbands, it would be clear that FMMTLD suggests a significant reduction in the computational complexity. This reduction in operations comes at the cost of restricting both denoising and mixing stages to use the same type of wavelet transform. Therefore, in case of using two different types of wavelet transforms, it is required to denoise all wavelet subbands (including the approximate and detail subbands) since the approximate subbands of these wavelet transforms are usually not the same.

## 4. Experimental Results

In this section, we present experimental results of the proposed multiscale TLD methods: MTLTLD, MMTLD, and FMMTLD. We compare the proposed methods with their single-scale baseline TLD method to show their effectiveness in exploiting multiscale nature of images. We describe the datasets and parameters which are used in our experiments. The qualitative and quantitative results are presented over classic test images and fluorescence microscopy images. The source code of our method will be made publicly available on the website <https://github.com/ashkan-abbasi66>.



Fig. 3: Classic test images. From left to right and top to bottom: *Barbara, Boat, Cameraman, Fingerprint, Gold hill, House, Lena, Living room, pirate, MRI, Parrots, Pentagon, Aerial, Building, Elaine, Starfish, Child, Saturn, Montage, and Einstein.*

### 4.1 The Datasets

Two datasets with different natures are used to evaluate the proposed methods. First, a collection of 20 classic test images are used to show the performance of the proposed methods in removing synthetic Gaussian noise. These images (Fig. 3) are quite general (including natural, medical, aerial and astronomical images), and they are frequently used in the image restoration and compression literature [28–30]. We corrupt these images by adding white Gaussian noise with three standard deviations (15, 25, and 50). We also used two more images only for illustration purposes in Fig. 2 and Fig. 4 (a).

The second dataset is a collection of microscopy images which are used to evaluate the performance of the proposed methods in solving an instance of a real world image denoising problem. We use the mixed test set from the recently published Fluorescence Microscopy Denoising (FMD) dataset [25]. These images are captured with three commercial microscopy imaging modalities (confocal, two-photon, and wide-field) from three representative biological samples (zebrafish embryo, fixed bovine pulmonary artery endothelial (BPAE) cells, and mouse brain tissues), and they are inherently corrupted by real Poisson-Gaussian noise. The images captured from BPAE cells are multi-channel (color). The other images are gray-scale. The whole set consists of five subsets with different noise levels. The first subset contains real noisy images, and the others were obtained by averaging 2, 4, 8, and 16 noisy images from the same field of view, respectively. Each subset has 48 noisy images. In addition to these five noisy subsets, there is a subset comprising of ground-truth images (each image is obtained by averaging 50 noisy images) which are mainly beneficial for quantitative evaluation of the performance of denoising methods.

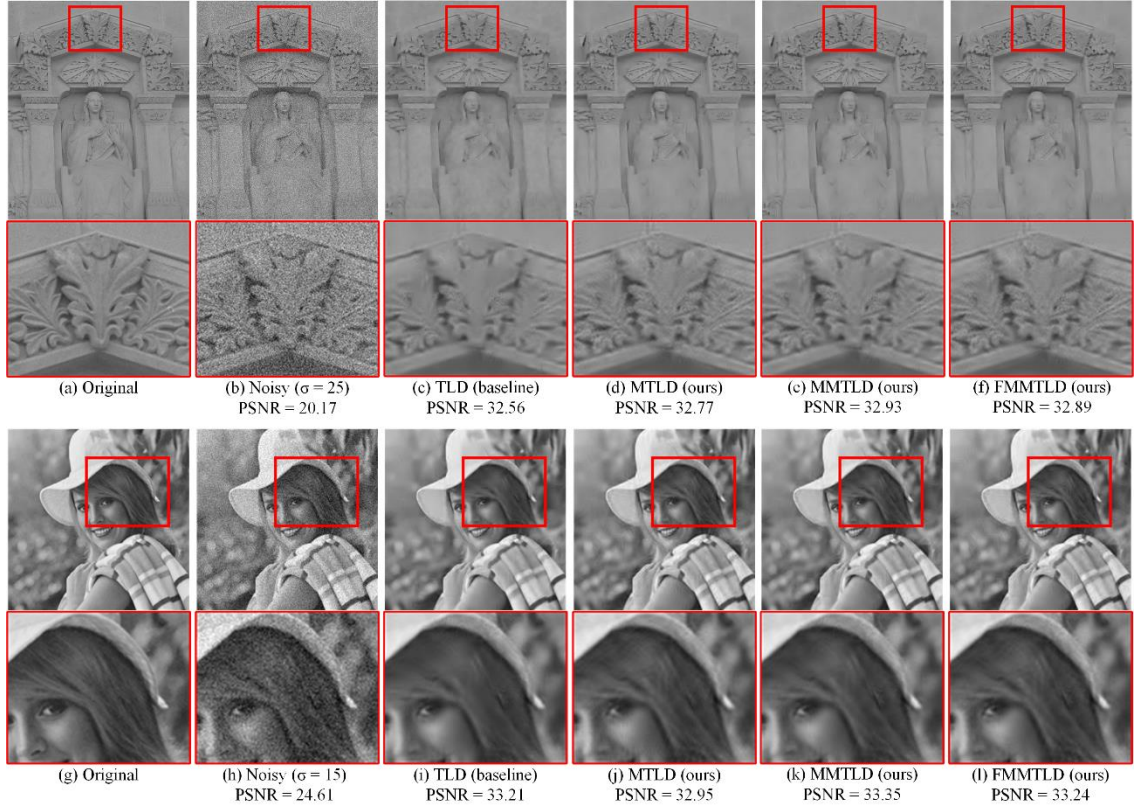


Fig. 4: Visual comparison of denoising results by the base line TLD method and the proposed multiscale methods (MTLD, MMTLD, and FMMTLD). The original image in (a) is *Fourvière Cathedral, north face* (from photo courtesy of F. A. P. Petitcolas).

## 4.2 The Parameters of Methods

The type of wavelet transform for implementing the three proposed multiscale methods (MTLD, MMTLD, and FMMTLD) can be considered as an important hyper-parameter. The wavelet transform comes in several forms. We can choose a critically-sampled or redundant wavelet transform. In addition to its type, the filterbank also plays an important role. Choosing the best wavelet transform or filterbank for implementing each method is beyond the scope of this paper. Therefore, while various wavelet transforms can be used to realize the proposed methods, we here restrict ourselves with the following simple configurations.

In our investigations, we implement the methods by substituting the “WT” and “WT<sub>x</sub>” modules in Fig. 1 with a 1-scale ( $J=1$ ) discrete wavelet transform (DWT) [2] and a 1-scale ( $K=1$ ) isotropic undecimated wavelet transform (IUWT) [31], respectively. Therefore, the denoising stages in all of the proposed methods are implemented with DWT, and we only use IUWT in the mixing stage of MMTLD. Note that, as it is stated in the previous section, if we use the same kind of wavelet transform for both the denoising and mixing stages in MMTLD, the method becomes equivalent to FMMTLD except that it has more computations. Thus, we intentionally use a different type of wavelet transform for the mixing stage of MMTLD to avoid getting similar results and show that the type of wavelet transform in this stage may have a significant role in the quality of outputs.

We use the discrete Meyer filterbank (MATLAB® “dmey”) to implement DWT. For denoising classic test images, we implement IUWT using the Astro filterbank [31] for which the vector of 1-D low-pass filter coefficients is  $[1, 4, 6, 4, 1]/16$ . The 2-D low-pass filter is obtained with the outer product of the 1-D low-pass filter by itself. Because the IUWT computes detail coefficients by subtraction of the current coarse image from the last fine image, it is not required to determine the high-pass filter coefficients. In our experiments, we found that the Astro filterbank is not suitable for analyzing fluorescence microscopy images and it results in over smoothing. Thus, for denoising these images, we implement IUWT using the Cohen-Daubechies-Fauveau 7/9 filterbank which is also shown to be useful for denoising [32]. In this filterbank, the vector of 1-D low-pass filter coefficients is  $[0, -0.04563588155, -0.02877176311, 0.295635881557, 0.557543526229, 0.295635881557, -0.02877176311, -0.04563588155, 0]$ .

Here, the baseline method (TLD) is a single-scale patch-based denoising method. We use TLD with patches of size  $11 \times 11$  pixels. All of the other parameters of TLD, except the constant  $c$  (Section 2.2), are set as described in [7]. This constant determines the sparsity level in the variable sparsity update. We use its default value (1.04) [7] for denoising classic test images, and set it to 0.9 for denoising microscopy images. Note that since these images were captured with different imaging modalities, the optimal approach is to treat each noise level and each imaging modality separately. However, to keep it simple and comply with [25], we do not employ this procedure.

### 4.3 Results for Gaussian Image Denoising

Fig. 2, and 4 show some visual comparisons between the denoising outputs of the three proposed multiscale methods (MTLD, MMTLD, and FMMTLD) and the baseline method (TLD). The input images are corrupted with three different levels of additive white Gaussian noise.

In Fig. 2, the input image is corrupted with a relatively strong ( $\sigma=50$ ) noise. It can be seen that TLD removes noise while it leaves a significant negative effect on the low-frequency structure of the image. A rectangular region from the damaged building façade in Fig. 2 (c) is magnified in Fig. 2 (i). Comparing Fig. 2 (i) and Fig. 2 (j) show that almost all of the damaged parts in Fig. 2 (i) are recovered by MTLD in Fig. 2 (j).

This is because MTLD is multiscale and one is expected that it has better denoising quality than its baseline. However, unlike what is expected, the lower PSNR value of MTLD (Fig. 2 (d)) compared to PSNR value of TLD (Fig. 2 (c)) reveals that MTLD suffer from another issue. As discussed in Section 3, the artifacts are responsible for this issue. In terms of presence of artifacts, it can be seen that MMTLD (Fig. 2 (e)) has the least amount of artifacts among all other denoising methods while the edges and low-frequency image structures are well recovered. The quality of FMMTLD’s output (Fig. 2 (f)) is slightly worse than the output of MMTLD. However, it has better performance than corresponding TLD and MTLD outputs.

There is a notable difference between the outputs of the proposed mixing based methods (Fig. 2 (e) and Fig. 2 (f)). This difference

TABLE I  
MEAN OF THE PSNR (DB) RESULTS FOR DENOISING 20 CLASSIC TEST  
IMAGES (FIG. 3) BY THE COMPARED METHODS. THE BEST RESULT IS SHOWN IN  
**BOLD** AND THE SECOND BEST RESULT IS UNDERLINED.

Method	Noise level ( $\sigma$ )			Average
	15	25	50	
Noisy Images	24.61	20.17	14.15	19.65
TLD (baseline)	32.81	30.11	26.54	29.82
MTLD (ours)	32.59	30.05	26.65	29.76
MMTLD (ours)	<b>32.94</b>	<b>30.35</b>	<b>26.95</b>	<b>30.08</b>
FMMTLD (ours)	<u>32.84</u>	<u>30.25</u>	<u>26.87</u>	<u>29.99</u>

comes from the fact that MMTLD utilizes IUWT for its mixing stage (Section 0). IUWT preserves translation-invariance property [31]. In contrast, FMMTLD solely based on DWT. The lack of translation-invariance in DWT leads to some artifacts when an image is reconstructed after modification of its wavelet subbands. Therefore, MMTLD generally produces less artifacts than FMMTLD.

The input image in Fig. 4 (a) is corrupted with a medium noise level ( $\sigma = 25$ ). In contrast to Fig. 2, MTLD leads to higher PSNR value compared to its baseline. This is because this input image mainly contains carved stone textures at different scales, and thus multiscale processing of this image is beneficial. Still, we can see that FMMTLD leads to better denoising quality than both TLD and MTLD due to attenuated artifacts by the mixing stage. A rectangular region from the top of the stone carved frame is magnified for each image. Comparing the magnified regions in Fig. 4 (d) and (f) verifies that the mixing stage in FMMTLD attenuates artifacts and preserves main image structures. Again, the best result is obtained using MMTLD.

In Fig. 4 (g), the Elaine test image is corrupted with a relatively low noise level ( $\sigma = 15$ ). In general, multiscale denoising is not beneficial in relatively low noise levels ( $\sigma < 25$ ) [9]. However, it can be seen that both of the MMTLD (Fig. 4 (k)) and FMMTLD (Fig. 4 (l)) outputs are quantitatively and qualitatively better than TLD (Fig. 4 (i)). Conversely, the MTLD output (Fig. 4 (j)) is significantly inferior to TLD's output. The reason is that in the low noise regimes artifacts produced through MTLD can prevail over the benefits of it. Thus, for low noise levels, the mixing stage is more advantageous in preserving the quality of image reconstruction at least as good as the single-scale baseline method.

The observations and explanations can be validated by the average quantitative results, tabulated in Table I and II. The average PSNR results are tabulated in Table I and the average of the structural similarity index (SSIM) [33] results are tabulated in Table II. These tables show that the two mixing based methods (MMTLD and FMMTLD) perform reasonably well in terms of both PSN

TABLE II  
 MEAN OF THE SSIM RESULTS FOR DENOISING 20 CLASSIC TEST IMAGES  
 (FIG. 3) BY THE COMPARED METHODS. THE BEST RESULT IS SHOWN IN **BOLD**  
 AND THE SECOND BEST RESULT IS UNDERLINED.

Method	Noise level ( $\sigma$ )			Average
	15	25	50	
Noisy Images	0.5128	0.3341	0.1532	0.3334
TLD (baseline)	0.8799	0.8148	0.6929	0.7959
MTLD (ours)	0.8784	0.8135	0.6781	0.7900
MMTLD (ours)	<b>0.8871</b>	<b>0.8292</b>	<b>0.7192</b>	<b>0.8118</b>
FMMTLD	<u>0.8843</u>	<u>0.8247</u>	<u>0.7116</u>	<u>0.8069</u>
(ours)				

-R and SSIM metrics. Also, these results confirm that MTLD is generally inferior to TLD because it produces considerable artifacts.

#### 4.4 Results for Real Fluorescence Microscopy Image Denoising

In this section, we show the efficiency of the proposed methods in denoising real images from the FMD dataset which are inherently corrupted by real Poisson-Gaussian noise. Since the proposed multiscale methods extend the baseline TLD method which is basically a Gaussian denoising method, it is required to perform a Gaussianizing procedure on the corrupted images, i.e., reducing their noise to nearly additive Gaussian noise. To this end, we apply the following three step procedure which is commonly used in the literature: (i) Transform a given noisy image using the generalized Anscombe transformation designed for Poisson-Gaussian noise [34]. The noisy data after this transformation becomes approximately homoscedastic and Gaussian, (ii) Apply a Gaussian denoising method, and (iii) Transform back the denoised data using an appropriate inverse transform. We here use the exact unbiased inverse transformation [35]. Some visual comparisons of the fluorescence microscopy image denoising results through the baseline method and the three proposed multiscale methods are shown in Fig. 5 and Fig. 6.

In Fig. 5, we show the results of denoising two representative single-channel fluorescence microscopy images (Fig. 5 (b) and (h)). The first row contains the ground-truth, noisy input, and denoising outputs corresponding to the Zebrafish embryo sample under confocal microscopy. The zoomed regions, in the second row, clearly show that the single-scale TLD method destroys edges and textures while the proposed multiscale methods results in the outputs that are more visually pleasing. Comparing Fig. 5 (d)-(f), it can be seen that the best denoising results are given by the two mixing based methods (MMTLD and FMMTLD). The PSNR values show that the MMTLD and FMMTLD results are very close to each other. Similar explanations can be made for describing the denoising results of the input image (Fig. 5 (h)) from the mouse brain tissues under two-photon microscopy. These results are



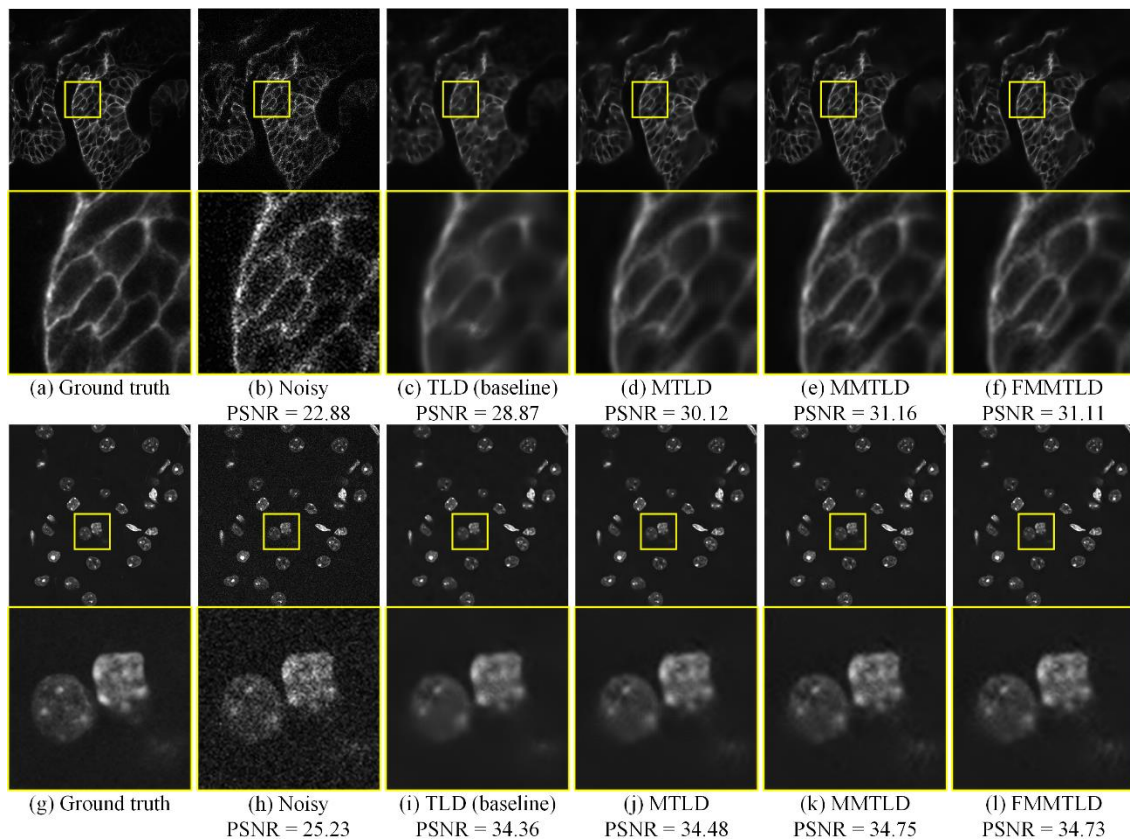


Fig. 5: Visual comparison of denoising results by the single-scale baseline TLD method and the proposed multiscale methods (MTLD, MMTLD, and FMMTLD). The images are gray-scale. In the 1<sup>st</sup> row, the output results of denoising a real noisy image from the Zebrafish embryo sample under confocal microscopy are shown. In the 3<sup>rd</sup> row, the output results of denoising a real noisy image from the mouse brain tissues under two-photon microscopy are shown. For each image, the boxed region is magnified below it. This figure is better observed by zooming on a computer screen.

shown in Fig. 5 (i)-(l). One can visually confirm that the brain cell structures in the zoomed regions are better recovered through the proposed multiscale mixing based methods. The recovery quality of both MMTLD and FMMTLD are almost the same.

In Fig. 6, we show the results of denoising two representative multi-channel (color) fluorescence microscopy images (Fig. 6 (b) and (h)). Each channel is independently denoised through the compared methods. The original noisy images are captured from the samples of BPAE cells under confocal (Fig. 6 (b)) and two-photon microscopy (Fig. 6 (h)). Comparing the results of TLD and MTLD for both input images show that although MTLD can reveal more structures, the PSNR values are nearly the same. As we have seen in the case of Gaussian denoising (e.g., Fig. 2 (i) and (j)), this is due to the existence of high-frequency artifacts in the MTLD results. This shortcoming is again resolved by the mixing stage in the MMTLD and FMMTLD methods. Their results are shown in the two rightmost columns in Fig. 6.

In case of denoising classic test images (Section **Error! Reference source not found.**), it is qualitatively and quantitatively confirmed that MTLD is inferior to the baseline TLD method. The presence of artifacts cancels out the benefits of recovering structures by MTLD. However, for the fluorescence microscopy images, Fig. 5 and Fig. 6 suggest that MTLD can produce better (or at least comparable) results than TLD. This can be validated with computing the quantitative metrics over the whole dataset.

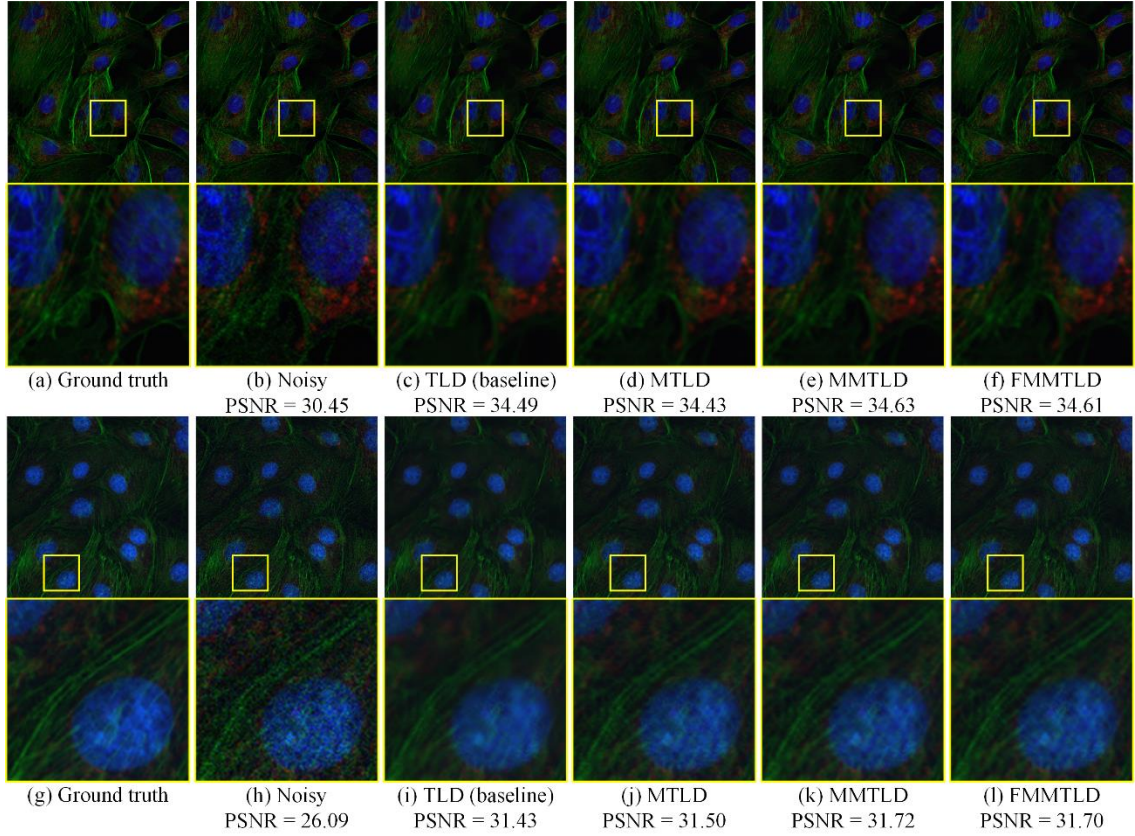


Fig. 6: Visual comparison of denoising results by the baseline TLD method and the proposed multiscale methods (MTLD, MMTLD, and FMMTLD). The images are multi-channel. In the 1<sup>st</sup> row, the output results of denoising a real noisy image from the BPAE cells under confocal microscopy are shown. In the 3<sup>rd</sup> row, the output results of denoising a real noisy image from the BPAE cells under two-photon microscopy are shown. For each image, the boxed region is magnified below it. This figure is better observed by zooming on a computer screen.

The average of PSNR and SSIM results are tabulated in Table III and IV, respectively. For each method in both of these tables, the average metric values are reported in the five columns. These columns are corresponding to the five subsets of images in the FMD dataset. From left to right, the noise level decreases since more images are averaged to obtain every image in the associated subset. Thus, the only first column is associated with the real noisy images which have the highest noise level. The tables show that MTLD is about 0.2 dB better than TLD over the first subset. This shows that multiscale denoising have a positive contribution for these types of images. It is expected that decreasing the noise level negatively affects the quality of multiscale denoising [9]. These tables also show that the superiority of MTLD over TLD is preserved just in the first two columns. For the other columns, the performance of MTLD is slightly inferior to TLD. In contrast, the two proposed multiscale mixing based methods (MMTLD and FMMTLD) are better than TLD even for the low noise regimes. Both MMTLD and FMMTLD are about 0.1 dB better than TLD for the last column (the subset of images with the lowest noise level). It is also worth to mention that, contrary to the obtained results in Gaussian denoising, the denoising results of fluorescence microscopy images through MMTLD and FMMTLD are very close to each other while FMMTLD has much less computation. The slightly



better performance of MMTLD can be contributed to the usage of IUWT (which is a redundant wavelet transform) in its mixing stage.

TABLE III  
MEAN OF THE PSNR RESULTS FOR DENOISING THE MIXED TEST SET FROM  
FMD DATASET THROUGH THE COMPARED METHODS. THE BEST RESULT IS  
SHOWN IN **BOLD** AND THE SECOND BEST RESULT IS UNDERLINED.

Method	Number of Images for Averaging				
	1	2	4	8	16
Noisy Images	27.22	30.08	32.86	36.03	39.70
TL (baseline)	32.13	33.83	35.95	38.01	40.66
MTLD (ours)	32.33	33.89	35.90	37.91	40.50
MMTLD (ours)	<b>32.39</b>	<b>33.93</b>	<b>35.97</b>	<b>38.07</b>	<b>40.75</b>
FMMTLD (ours)	<u>32.36</u>	<u>33.92</u>	<u>35.96</u>	<u>38.06</u>	<u>40.74</u>

#### 4.5 Runtimes of the compared methods

All of the compared methods are implemented in MATLAB. It has been demonstrated that TLD is notably faster than K-SVD denoising [6–8]. The sparse coding problem in TLD is much simpler than the one in K-SVD denoising. Consequently, each iteration for the transform learning is faster than the synthesis K-SVD [4,5]. We can summarize the key computations involved in the proposed multiscale methods (Fig. 1) as follows. Applying wavelet transform, inverse wavelet transform, and TLD. From these operations, the most costly one is TLD.

If we use a  $J$ -scale wavelet transform in MTLD, the method runs TLD to denoise  $3J + 1$  wavelet subbands. With decimated wavelet transforms, the wavelet subbands are smaller than the input image. Therefore, it is expected that the multiscale denoising through MTLD does not significantly increase the overall computations. As an example, if we use a 1-scale ( $J=1$ ) DWT to implement MTLD, the method requires to denoise 4 wavelet subbands, each one having one-fourth size of the input image. Thus, the computational complexity of denoising a given input image through 1-scale MTLD is theoretically the same as TLD. However, in practice, the TLD method’s runtime not only depends on the size of its input image but also on its content and noise level. In fact, the number of iterations for the variable sparsity update step in TLD varies for different input images or noise levels. As mentioned in Section 2.2, this step increments sparsity by one at a time until a predetermined error threshold is met for all patches. For example, it is reported in [7] that TLD denoises the Cameraman image faster than the Barbara image

TABLE IV  
 MEAN OF THE SSIM RESULTS FOR DENOISING THE MIXED TEST SET FROM  
 FMD DATASET THROUGH THE COMPARED METHODS. THE BEST RESULT IS  
 SHOWN IN **BOLD** AND THE SECOND BEST RESULT IS UNDERLINED.

Method	Number of Images for Averaging				
	1	2	4	8	16
Noisy Images	0.5442	0.6800	0.7981	0.8892	0.9487
TLD (baseline)	0.7796	0.8379	0.8958	0.9344	0.9608
MTLD (ours)	0.7828	0.8392	0.8950	0.9336	0.9603
MMTLD (ours)	<b>0.7858</b>	<b>0.8408</b>	<b>0.8961</b>	<b>0.9352</b>	<b>0.9620</b>
FMMTLD (ours)	<u>0.7853</u>	<u>0.8405</u>	<u>0.8959</u>	<u>0.9350</u>	<u>0.9618</u>

since the error threshold for the Cameraman image satisfies sooner.

In Table V, we report runtimes for denoising the Barbara image corrupted with the three levels of additive white Gaussian noise through the compared methods. The entries in Table V are rounded to the nearest integer. Note how the Gaussian noise level has a notable impact on the overall runtime. The bigger the noise level, the bigger the error threshold (Section 2.2) which satisfies sooner. This table also shows that the runtime of MTLD is significantly higher than TLD. This is in contrast to what is expected since the same number of pixels are processed by those methods. The reason lies in the different convergence behaviors. The baseline TLD method denoises the input image while MTLD denoises all of the wavelet subbands of the input image. In Table V, we report runtimes for denoising the Barbara image corrupted with the three levels of additive white Gaussian noise through the compared methods. The entries in Table V are rounded to the nearest integer. Note how the Gaussian noise level has a notable impact on the overall runtime. The bigger the noise level, the bigger the error threshold (Section 2.2) which satisfies sooner. This table also shows that the runtime of MTLD is significantly higher than TLD. This is in contrast to what is expected since the same number of pixels are processed by those methods. The reason lies in the different convergence behaviors. The baseline TLD method denoises the input image while MTLD denoises all of the wavelet subbands of the input image.

MMTLD combines the results of MTLD and TLD. Therefore, the runtime of MMTLD is at least equal to the sum of the runtimes of TLD and MTLD. Table V shows that the computation time of the other operations (which we propose to combine the results in MMTLD) takes less than one second. In FMMTLD, the method only denoises the input image and its approximate subband at scale  $J$ . Thus, FMMTLD provides significant speedup compared to the other two multiscale methods while its

reconstruction quality is better than MTLD and slightly inferior to MMTLD. Especially, as we have shown in Section 4.4, FMMTLD has close performance to MMTLD in case of denoising fluorescence microscopy images.

TABLE V  
RUNTIMES (IN SECONDS) FOR APPLYING THE COMPARED METHODS ON THE  
*Barbara* IMAGE WITH SIZE 512X512 PIXELS. THE INPUT IMAGE IS CORRUPTED  
WITH DIFFERENT LEVELS OF ADDITIVE WHITE GAUSSIAN NOISE.

Noise level ( $\sigma$ )	TLD	MTLD	MMTLD	FMMTLD
15	63	183	246	141
25	52	152	204	116
50	42	125	167	93

## 5. Conclusion

Sparsifying transform learning is a data-driven sparse model that can be efficiently used for adaptive image denoising [6–8]. However, similar to other data-driven sparse models, it is intrinsically single-scale. To exploit the multiscale nature of images in the transform learning denoising (TLD), this paper investigates several methods. Specifically, three multiscale denoising methods are proposed, namely MTLD, MMTLD, and FMMTLD. In multiscale TLD (MTLD), the method simply denoises all wavelet subbands through TLD. This approach is simple and intuitive but it produces artifacts. Moreover, it is computationally demanding since it needs to denoise every wavelet subbands. To suppress these artifacts, we utilize the wavelet subbands mixing [21,22] which is a cheap fusion technique. In the mixed MTLD (MMTLD), the method combines the results of the single-scale (TLD) and multiscale (MTLD) methods. Experiments show that MMTLD can preserve image structures while greatly suppress artifacts. However, its computational cost is greater than MTLD. We show that in order to significantly reduce the computational cost of MMTLD, we can use the same wavelet transform in both of the denoising and mixing stages. This simplification leads to another method which is called fast MMTLD (FMMTLD). The main property of FMMTLD is that the method saves computations required to denoise detail subbands, leading to a simpler multiscale denoising method. Extensive experiments are performed over two datasets: classic test images corrupted with Gaussian noise and fluorescence microscopy images corrupted with real Poisson-Gaussian noise. These experiments show that the proposed mixing based multiscale denoising methods (MMTLD and FMMTLD) are capable of recovering underlying image details and greatly suppress artifacts. The simplicity of FMMTLD suggests that it has a potential to be extended for three dimensional denoising. It is also worth to mention that the methods which are investigated here are not restricted to sparse models. In fact, these methods are quite

general and have a potential to enhance other single-scale denoising methods which are developed based on various models such as spatial filtering [36], variational approximations [37], nonlocal models [38], low-rank assumptions [39,40], tensor factorization [41], and deep neural networks [42]. We leave this as a promising direction for future researches.

## Acknowledgment

This paper was supported by the National Natural Science Foundation of China under Grant No.61922029, and the National Natural Science Foundation under Grant No. 61771192. The authors also would like to thank Prof. Ravishankar and his colleagues for making their source code freely available.

## References

- [1] N. Ahmed, T. Natarajan, K. Rao, Discrete Cosine Transform, *IEEE Trans. Comput.* C-23 (1974) 90–93. <https://doi.org/10.1109/T-C.1974.223784>.
- [2] S. Mallat, *A wavelet tour of signal processing*, Elsevier, 1999.
- [3] B.A. Olshausen, D.J. Field, Emergence of simple-cell receptive field properties by learning a sparse code for natural images, *Nature*. 381 (1996) 607–609. <https://doi.org/10.1038/381607a0>.
- [4] M. Aharon, M. Elad, A. Bruckstein, K-SVD: An algorithm for designing overcomplete dictionaries for sparse representation, *IEEE Trans. Signal Process.* 54 (2006) 4311–4322. <https://doi.org/10.1109/TSP.2006.881199>.
- [5] M. Elad, M. Aharon, Image Denoising Via Sparse and Redundant Representations Over Learned Dictionaries, *IEEE Trans. Image Process.* 15 (2006) 3736–3745.
- [6] S. Ravishankar, Y. Bresler, Learning Sparsifying Transforms, *IEEE Trans. Signal Process.* 61 (2013) 1072–1086. <https://doi.org/10.1109/TSP.2012.2226449>.
- [7] S. Ravishankar, Y. Bresler, Learning Doubly Sparse Transforms for Images, *IEEE Trans. Image Process.* 22 (2013) 4598–4612. <https://doi.org/10.1109/TIP.2013.2274384>.
- [8] S. Ravishankar, Y. Bresler, Sparsifying Transform Learning With Efficient Optimal Updates and Convergence Guarantees, *IEEE Trans. Signal Process.* 63 (2015) 2389–2404. <https://doi.org/10.1109/TSP.2015.2405503>.
- [9] M. Lebrun, M. Colom, A. Buades, J.M. Morel, Secrets of image denoising cuisine, *Acta Numer.* 21 (2012) 475–576. <https://doi.org/10.1017/S0962492912000062>.
- [10] B.A. Olshausen, P. Sallee, M.S. Lewicki, Learning sparse image codes using a wavelet pyramid architecture, in: *Adv. Neural Inf. Process. Syst.*, 2001: pp. 887–893.

- [11] P. Sallee, B.A. Olshausen, Learning sparse multiscale image representations, in: *Adv. Neural Inf. Process. Syst.*, 2003: pp. 1351–1358.
- [12] S. Bacchelli, S. Papi, Image denoising using principal component analysis in the wavelet domain, *J. Comput. Appl. Math.* 189 (2006) 606–621. <https://doi.org/10.1016/j.cam.2005.04.030>.
- [13] J. Mairal, G. Sapiro, M. Elad, Learning Multiscale Sparse Representations for Image and Video Restoration, *Multiscale Model. Simul.* 7 (2008) 214–241. <https://doi.org/10.1137/070697653>.
- [14] B. Ophir, M. Lustig, M. Elad, Multi-Scale Dictionary Learning Using Wavelets, *IEEE J. Sel. Top. Signal Process.* 5 (2011) 1014–1024. <https://doi.org/10.1109/JSTSP.2011.2155032>.
- [15] L. Fang, S. Li, Q. Nie, J.A. Izatt, C.A. Toth, S. Farsiu, Sparsity based denoising of spectral domain optical coherence tomography images., *Biomed. Opt. Express.* 3 (2012) 927–42. <https://doi.org/10.1364/BOE.3.000927>.
- [16] R. Yan, L. Shao, Y. Liu, Nonlocal Hierarchical Dictionary Learning Using Wavelets for Image Denoising, *IEEE Trans. Image Process.* 22 (2013) 4689–4698. <https://doi.org/10.1109/TIP.2013.2277813>.
- [17] J. Sulam, B. Ophir, M. Elad, Image denoising through multi-scale learnt dictionaries, in: *IEEE Int. Conf. Image Process.*, IEEE, 2014: pp. 808–812. <https://doi.org/10.1109/ICIP.2014.7025162>.
- [18] J.M. Hughes, D.N. Rockmore, Y. Wang, Bayesian Learning of Sparse Multiscale Image Representations, *IEEE Trans. Image Process.* 22 (2013) 4972–4983. <https://doi.org/10.1109/TIP.2013.2280188>.
- [19] P. Burt, E. Adelson, The Laplacian Pyramid as a Compact Image Code, *IEEE Trans. Commun.* 31 (1983) 532–540. <https://doi.org/10.1109/TCOM.1983.1095851>.
- [20] N. Yu, T. Qiu, F. Ren, Denoising for Multiple Image Copies through Joint Sparse Representation, *J. Math. Imaging Vis.* 45 (2013) 46–54. <https://doi.org/10.1007/s10851-012-0343-1>.
- [21] A. Lukin, A Multiresolution Approach for Improveing Quality of Image Denoising Algorithms, in: *IEEE Int. Conf. Acoust. Speed Signal Process. Proc.*, IEEE, 2006: pp. II-857–II-860. <https://doi.org/10.1109/ICASSP.2006.1660478>.
- [22] P. Coupé, P. Hellier, S. Prima, C. Kervrann, C. Barillot, 3D Wavelet Subbands Mixing for Image Denoising, *Int. J. Biomed. Imaging.* 2008 (2008) 1–11. <https://doi.org/10.1155/2008/590183>.
- [23] T. Plotz, S. Roth, Benchmarking denoising algorithms with real photographs, in: *IEEE Conf. Comput. Vis. Pattern Recognit.*, 2017: pp. 1586–1595.
- [24] A. Abdelhamed, S. Lin, M.S. Brown, A high-quality denoising dataset for smartphone cameras, in: *IEEE Conf. Comput. Vis. Pattern Recognit.*, 2018: pp. 1692–1700.
- [25] Y. Zhang, Y. Zhu, E. Nichols, Q. Wang, S. Zhang, C. Smith, S. Howard, A Poisson-Gaussian Denoising Dataset With

- Real Fluorescence Microscopy Images, in: IEEE Conf. Comput. Vis. Pattern Recognit., IEEE, 2019: pp. 11702–11710. <https://doi.org/10.1109/CVPR.2019.01198>.
- [26] B. Brummer, C. De Vleeschouwer, Natural Image Noise Dataset, in: IEEE Conf. Comput. Vis. Pattern Recognit. Work., 2019: p. 0.
- [27] R. Rubinstein, M. Zibulevsky, M. Elad, Double Sparsity: Learning Sparse Dictionaries for Sparse Signal Approximation, *IEEE Trans. Signal Process.* 58 (2010) 1553–1564. <https://doi.org/10.1109/TSP.2009.2036477>.
- [28] J. Portilla, V. Strela, M.J. Wainwright, E.P. Simoncelli, Image denoising using scale mixtures of Gaussians in the wavelet domain, *IEEE Trans. Image Process.* 12 (2003) 1338–1351. <https://doi.org/10.1109/tip.2003.818640>.
- [29] V. Pappyan, M. Elad, Multi-Scale Patch-Based Image Restoration, *IEEE Trans. Image Process.* 25 (2016) 249–261. <https://doi.org/10.1109/TIP.2015.2499698>.
- [30] W. Dong, G. Shi, Y. Ma, X. Li, Image Restoration via Simultaneous Sparse Coding: Where Structured Sparsity Meets Gaussian Scale Mixture, *Int. J. Comput. Vis.* 114 (2015) 217–232. <https://doi.org/10.1007/s11263-015-0808-y>.
- [31] J.-L. Starck, J. Fadili, F. Murtagh, The Undecimated Wavelet Decomposition and its Reconstruction, *IEEE Trans. Image Process.* 16 (2007) 297–309. <https://doi.org/10.1109/TIP.2006.887733>.
- [32] J.-L. Starck, F. Murtagh, J. Fadili, Sparse image and signal processing: Wavelets and related geometric multiscale analysis, Cambridge university press, 2015.
- [33] Z. Wang, A.C. Bovik, H.R. Sheikh, E.P. Simoncelli, Image Quality Assessment: From Error Visibility to Structural Similarity, *IEEE Trans. Image Process.* 13 (2004) 600–612. <https://doi.org/10.1109/TIP.2003.819861>.
- [34] F. Murtagh, J.-L. Starck, A. Bijaoui, Image restoration with noise suppression using a multiresolution support., *Astron. Astrophys. Suppl. Ser.* 112 (1995) 179.
- [35] M. Makitalo, A. Foi, Optimal Inversion of the Generalized Anscombe Transformation for Poisson-Gaussian Noise, *IEEE Trans. Image Process.* 22 (2013) 91–103. <https://doi.org/10.1109/TIP.2012.2202675>.
- [36] T.F. Chan, J.J. Shen, Image processing and analysis: variational, PDE, wavelet, and stochastic methods, Siam, 2005.
- [37] A. Beck, M. Teboulle, Fast Gradient-Based Algorithms for Constrained Total Variation Image Denoising and Deblurring Problems, *IEEE Trans. Image Process.* 18 (2009) 2419–2434. <https://doi.org/10.1109/TIP.2009.2028250>.
- [38] A. Buades, B. Coll, J.-M. Morel, A Non-Local Algorithm for Image Denoising, in: IEEE Conf. Comput. Vis. Pattern Recognit., IEEE, 2005: pp. 60–65. <https://doi.org/10.1109/CVPR.2005.38>.
- [39] W. Dong, G. Shi, X. Li, Nonlocal image restoration with bilateral variance estimation: A low-rank approach, *IEEE Trans. Image Process.* 22 (2013) 700–711. <https://doi.org/10.1109/TIP.2012.2221729>.

- [40] S. Gu, Q. Xie, D. Meng, W. Zuo, X. Feng, L. Zhang, Weighted Nuclear Norm Minimization and Its Applications to Low Level Vision, *Int. J. Comput. Vis.* 121 (2017) 183–208. <https://doi.org/10.1007/s11263-016-0930-5>.
- [41] A. Rajwade, A. Rangarajan, A. Banerjee, Image Denoising Using the Higher Order Singular Value Decomposition, *IEEE Trans. Pattern Anal. Mach. Intell.* 35 (2013) 849–862. <https://doi.org/10.1109/TPAMI.2012.140>.
- [42] K. Zhang, W. Zuo, Y. Chen, D. Meng, L. Zhang, Beyond a Gaussian denoiser: Residual learning of deep CNN for image denoising, *IEEE Trans. Image Process.* 26 (2017) 3142–3155. <https://doi.org/10.1109/TIP.2017.2662206>.